JOURNAL OF COMPUTATIONAL PHYSICS 47, 412–433 (1982)

Solution of the Schrödinger Equation by a Spectral Method*

M. D. FEIT, J. A. FLECK, JR., AND A. STEIGER

University of California, Lawrence Livermore National Laboratory, Livermore, California 94550

Received February 10, 1982

A new computational method for determining the eigenvalues and eigenfunctions of the Schrödinger equation is described. Conventional methods for solving this problem rely on diagonalization of a Hamiltonian matrix or iterative numerical solutions of a time independent wave equation. The new method, in contrast, is based on the spectral properties of solutions to the time-dependent Schrödinger equation. The method requires the computation of a correlation function $\langle \psi(\mathbf{r}, 0) | \psi(\mathbf{r}, t) \rangle$ from a numerical solution $\psi(\mathbf{r}, t)$. Fourier analysis of this correlation function reveals a set of resonant peaks that correspond to the stationary states of the system. Analysis of the location of these peaks reveals the eigenvalues with high accuracy. Additional Fourier transforms of $\psi(\mathbf{r},t)$ with respect to time generate the eigenfunctions. The effectiveness of the method is demonstrated for a one-dimensional asymmetric double well potential and for the two-dimensional Hénon–Heiles potential.

1. INTRODUCTION

The need for solving the Schrödinger equation numerically can arise in the description of nuclear motion in molecules in the Born–Oppenheimer approximation or in the description of atoms and molecules in self-consistent field approximations. For either application, the currently available numerical methods for solving the time-independent Schrödinger equation fall into two categories. Methods in the first category rely on matrix diagonalization and have as their starting point the representation of the wavefunction in terms of a finite set of basis functions [1–6]. The basis functions may be selected from a complete orthogonal set or they may be chosen for specific properties such as symmetry and spatial behavior. In either case, the diagonalization of a Hamiltonian matrix computed from the basis functions produces the desired eigenvalues and eigenfunctions. In the second category are the iterative methods that require repeated numerical integrations of the Schrödinger equation, accompanied by adjustments of the energy eigenvalues [7–9]. Typically, an eigenvalue is estimated initially, and the corresponding eigenfunction is computed by numerical integration. Knowledge of the eigenfunction enables the computation of an improved eigenvalue, which provides the input to the next iteration, and so on.

* Work performed under the auspices of the U. S. Department of Energy by the Lawrence Livermore National Laboratory under contract No. W-7405-ENG-48.

0021-9991/82/090412–22$02.00/0

Matrix diagonalization is attractive for treating Hamiltonians that do not differ greatly from Hamiltonians with known eigenfunctions or for potentials with simple analytic forms, which permit setting up the Hamiltonian matrix without excessive computation. Matrix diagonalization becomes less attractive when a large amount of computation is required to set up the Hamiltonian matrix or, in general, when the required Hamiltonian matrix is of high order. The iterative numerical integration methods are known to give very accurate results for one-dimensional problems. To apply them, it is necesssary to home in on the individual eigenvalues before the cycle of iterations is begun, both to reduce the number of iterations and to assure that no eigenvalues are missed [8]. While this poses no problem in principle, it can lower efficiency in situations where information on the eigenvalue spectrum is limited. To our knowledge, no practical iterative numerical integration scheme has been developed for two dimensions.

In this paper we describe a new method for solving the Schrödinger eigenvalue problem, which utilizes numerical solutions to the time-dependent Schrödinger equation. The method is quite general and has, we believe, some special advantages for certain problems. The new method, which we shall call the spectral method, was developed earlier for determining the eigenvalues and eigenfunctions for the modes of optical waveguides from numerical solutions of the paraxial wave equation [10–13]. Since the latter equation is identical to the Schrödinger equation, it is possible to apply the previously developed methodology to quantum mechanical problems with little change.

The spectral method requires computation of the correlation function $\mathscr{S}_1(t) = \langle \psi(\mathbf{r}, 0) | \psi(\mathbf{r}, t) \rangle$, where $\psi(\mathbf{r}, t)$ represents a numerical solution to the time-dependent Schrödinger equation, and $\psi(\mathbf{r}, 0)$ is the wave function at $t = 0$. The solution $\psi(\mathbf{r}, t)$ can be accurately generated with the help of the split operator FFT method [14]. The numerical Fourier transform of $\mathscr{S}_1(t)$, or $\mathscr{S}_1(E)$, displays a set of sharp local maxima for $E = E_n$, where E_n are the desired energy eigenvalues. With the aid of lineshape fitting techniques, both the positions and heights of these resonances can be determined with high accuracy. The former yield the eigenvalues and the latter the weights of the stationary states that compose the wave packet. Once the eigenvalues are known, the corresponding eigenfunctions can be computed by numerically evaluating the integrals

$$\psi(\mathbf{r}, E_n) = \int_0^T \psi(\mathbf{r}, t)\, w(t) \exp(iE_n t)\, dt, \tag{1}$$

where T is the time encompassed by the calculation, and $w(t)$ is a window function.

An attractive feature of this method is that it allows the eigenvalue spectrum to be displayed graphically and the energy levels to be identified visually as they would be from an experimentally determined spectrum. Since the lineshapes for the theoretical spectrum are known, it is also possible to characterize the spectrum quantitatively.

The spectral method is in principle applicable to any linear eigenvalue problem [15] and to problems involving any number of dimensions. The only essential is an

available numerical solution for the time-dependent wavefunction (or other dependent variable) specified on a suitable coordinate grid. The high accuracy of the split operator FFT method [14] makes it particularly attractive for application with the spectral method to the Schrödinger equation in Cartesian coordinates.

Since the spectral method is fundamentally based on numerical solutions to a time-dependent differential equation, its implementation is always straightforward. No special ad hoc selection of basis functions is required, nor is it necessary for the potential to have a special analytic form. The only requirement for accuracy is the specification of adequate sampling rates in space and time for the numerical solution. Criteria for these sampling rates are simply related to the Nyquist sampling rates used in digital signal analysis. The accuracy of matrix diagonalization techniques, on the other hand, can be influenced by the specific choice of basis functions, and the amount of computation to set up the Hamiltonian matrix will vary strongly with both the basis set and the potential.

In this paper, we describe the application of the spectral method to the solution of the Schrödinger equation in either one or two Cartesian coordinates, and we provide results for two representative potentials, the 1-D asymmetric double well potential [2, 16, 17] and the Hénon–Heiles potential [3, 4–6], which has received considerable attention in studies of quantum ergodicity. Generalization of the method to three Cartesian coordinates, however, is both straightforward and feasible for some current generation computers. Results for three-dimensional computations will be described in subsequent publications. For further applications and accuracy tests of the spectral method, the reader is referred to [10–15].

The paper is organized as follows: In Section 2, the split operator FFT method for solving the time-dependent Schrödinger equation is reviewed, and accuracy criteria are established for picking the time increment Δt and the number of increments to be used in the temporal advance of the solution. In Section 3, the computation of a correlation function from the numerical solution for $\psi(x, y, t)$ is described. From a finite record of this correlation function, a Fourier energy spectrum can be constructed with the help of a window function. An analysis of the resonant line structure of this spectrum in turn yields the eigenvalues. In Section 4, it is shown how the eigenfunctions can be generated by computing additional Fourier transforms of $\psi(x, y, t)$ with respect to time. Results for the asymmetric double well potential are presented in Section 5, and results for the Hénon–Heiles potential in Section 6.

2. Solution Method for the Schrödinger Equation

We shall be concerned in this paper with solutions to the Schrödinger equation in two Cartesian coordinates, which in dimensionless form is

$$i\frac{\partial \psi}{\partial t} = -\frac{1}{2M}\nabla^2\psi + V(x, y)\psi, \tag{2}$$

where

$$\nabla^2 = \frac{\partial^2}{\partial x^2} + \frac{\partial^2}{\partial y^2}. \tag{3}$$

We review briefly the symmetrically split operator algorithm for advancing the solution to Eq. (2) by an incremental time Δt. This can be expressed formally as

$$\psi(x, y, t_0 + \Delta t) = \exp((i\,\Delta t/4M)\,\nabla^2)\exp(-i\,\Delta t V)\exp((i\,\Delta t/4M)\,\nabla^2)\,\psi(x, y, t_0) + O[(\Delta t)^3] \tag{4}$$

In Eq. (4), commutation errors give rise to the third order term in Δt, and the operator

$$\exp((i\,\Delta t/4M)\,\nabla^2) \tag{5}$$

applied to $\psi(x, y, t_0)$ is equivalent to solving the free particle wave equation

$$i\frac{\partial \psi}{\partial t} = -\frac{1}{2M}\left(\frac{\partial^2 \psi}{\partial x^2} + \frac{\partial^2 \psi}{\partial y^2}\right) \tag{6}$$

over a time $\Delta t/2$, with $\psi(x, y, t_0)$ as the initial wavefunction at $t = t_0$. The solution to Eq. (6) is obtained with the help of the band-limited Fourier series representation

$$\psi(x, y, t) = \sum_{m=-N/2+1}^{N/2} \sum_{n=-N/2+1}^{N/2} \psi_{mn}(t) \exp\left[\frac{2\pi i}{L_0}(mx + ny)\right], \tag{7}$$

where

$$\psi_{mn}(t_0 + \Delta t) = \psi_{mn}(t_0)\exp[-(i\,\Delta t/2M)(2\pi/L_0)^2\,(m^2 + n^2)], \tag{6}$$

and L_0 is the length of a side of the square computational grid. The right-hand side of expression (4) is thus equivalent to free particle propagation over a half time increment, a phase change from the action of the potential applied over the whole time increment, and an additional free particle propagation over a half time increment. If many factors of the form (4) are applied in sequence, pairs of half-step free particle propagations combine into full-step propagations. The computation thus proceeds as a succession of full-step propagations, applied in momentum space, alternating with phase changes of the wave function executed in configuration space. The only exceptions to this rule are the half steps of propagation applied at the beginning and end of the calculation.

This procedure is very efficient, when implemented with the help of the fast Fourier transform (FFT) algorithm, and very accurate, since, as is well known, the spatial derivatives are approximated to Nth order in L_0/N, where N is the number of grid points along a grid line and $\Delta x = \Delta y = L_0/N$ is the grid spacing. The grid length

L_0 must be chosen sufficiently large that the wavefunction is negligible on the grid boundary. The spatial sampling interval Δx must be chosen small enough to accommodate the spatial bandwidth of the wavefunction. This can be assured by monitoring the Fourier coefficients ψ_{mn} and determining that they are small on the boundaries of the grid in reciprocal space.

The time increment or sampling interval Δt must be chosen small enough to assure accurate computation of the time-dependent wavefunction. The overriding criterion for this selection is based on the width of the energy spectrum, determined by the Fourier transform of $\langle \psi(x, y, 0) | \psi(x, y, t) \rangle$. The sampling interval Δt limits the spectral bandwidth of a function that can be represented by a Fourier series determined by sampled values. That maximum bandwidth is

$$\Delta E_{\max} = \pi / \Delta t. \tag{9}$$

The sampling interval Δt should therefore be chosen small enough to accommodate at least the entire spectrum of bound state energy levels or

$$\Delta t < \pi / \Delta V_{\max}, \tag{10}$$

where $\Delta V_{\max}$ is the maximum excursion of the potential. Failure to meet criterion (10) will result in aliasing errors. Excellent results are normally assured when

$$\Delta t < \pi / 3\, \Delta V_{\max}. \tag{11}$$

If the potential under consideration is unbounded, it will be necessary to apply an appropriate bound in order to apply the method.

If the wave function is generated over a total time T, the minimum separation in energy levels that can be resolved is

$$\Delta E_{\min} = \pi / T. \tag{12}$$

Equation (10) also provides an estimate of the accuracy with which individual eigenvalues can be determined from the numerically computed energy spectrum without the aid of lineshape fitting techniques. With the aid of such techniques, on the other hand, the accuracy of eigenvalue determination implied by Eq. (12) can be improved by roughly two orders of magnitude.

The excitation of energy eigenstates can be controlled by the selection of the initial wavefunction $\psi(x, y, 0)$. There are various reasons for wanting to control the presence of eigenstates in the wave packet. One practical reason is to avoid exciting states with energy eigenvalues close enough to make it difficult to resolve the corresponding spectral lines. It may also be useful to control the number of states excited at one time to facilitate their classification. The choice of the initial wavefunction for one or more of these purposes can normally be based upon symmetry considerations. The simplification of the energy spectra by specification of the symmetry of the initial wavefunction is analogous to simplification of the Hamiltonian matrix by applying group theory to the symmetry properties of the Hamiltonian.

3. Correlation Functions, Spectra, and Eigenvalue Determination

The solution to Eq. (2) can be expressed as a linear superposition of eigenfunctions,

$$\psi(x, y, t) = \sum_{n,j} A_{nj} u_{nj}(x, y,) \exp(-iE_n t), \tag{13}$$

where the index j is used to distinguish states within a degenerate set and $u_{nj}(x, y)$ satisfies

$$-(1/2M)\nabla^2 u_{nj} + V u_{nj} = E_n u_{nj}. \tag{14}$$

Let us define the correlation function $\mathscr{P}_1(t)$ as

$$\begin{aligned}\mathscr{P}_1(t) &= \langle \psi(x, y, 0) | \psi(x, y, t) \rangle \\ &= \iint \psi^*(x, y, 0)\, \psi(x, y, t)\, dx\, dy.\end{aligned} \tag{15}$$

If expression (13) is used in Eq. (15), the result is

$$\mathscr{P}_1(t) = \sum_{n,j} |A_{nj}|^2 \exp(-iE_n t). \tag{16}$$

The Fourier transform of Eq. (16) is

$$\mathscr{P}_1(E) = \sum_{n,j} |A_{nj}|^2\, \delta(E - E_n). \tag{17}$$

The presence of the δ-functions in Eq. (17) implies that an infinite length record of the correlation function $\mathscr{P}(t)$ is available. In practice, only a finite record of length T is available, either from observation or computation. We take account of this fact by multiplying the right-hand side of Eq. (16), before Fourier transforming, by the normalized Hanning window function $w(t)/T$, where

$$\begin{aligned} w(t) &= 1 - \cos(2\pi t/T), && \text{if} \quad 0 \leqslant t \leqslant T, \\ &= 0, && \text{if} \quad t > T. \end{aligned} \tag{18}$$

The result is

$$\mathscr{P}_1(E) = \sum_n W_n \mathscr{L}_1(E - E_n), \tag{19}$$

where the relative weights of the states are

$$W_n = \sum_j |A_{nj}|^2 \tag{20}$$

and the lineshape function $\mathscr{L}_1(E-E_n)$ is defined by

$$\mathscr{L}_1(E-E_n)=\frac{1}{T}\int_0^T \exp[i(E-E_n)t]\, w(t)\, dt$$
$$=\frac{\exp[i(E-E_n)T]-1}{i(E-E_n)T}-\frac{1}{2}\left[\frac{\exp\{i[(E-E_n)T+2\pi]\}-1}{i[(E-E_n)T+2\pi]}\right.$$
$$\left.+\frac{\exp\{i[(E-E_n)T-2\pi]\}-1}{i[(E-E_n)T-2\pi]}\right]. \tag{21}$$

Without the window function, the individual resonances would resemble the function $\sin(\frac{1}{2}(E-E_n)T)/(E-E_n)$, whose sidelobes might be confused with or overlap other resonances. Employing the window function (18) in the Fourier transform greatly reduces the amplitudes of these sidelobes and makes possible an accurate identification of the positions of the resonances.

The procedure for calculating eigenvalues is straightforward. The correlation function $\mathscr{P}_1(t)$ is evaluated numerically by trapezoidal integration for each time step, the Fourier transform $\mathscr{P}_1(E)$ is evaluated numerically from the sampled values of $\mathscr{P}_1(t)$ upon completion of the desired number of integration steps, and, finally, the data set for $\mathscr{P}_1(E)$ is fit to the form of (19). For most cases, excellent results are obtained by assuming a single-line fit or

$$\mathscr{P}_1(E)=W_n\mathscr{L}_1(E-E_n) \tag{22}$$

for $E\sim E_n$. Occasionally, when resonances overlap significantly, the accuracy of the weights W_n can be improved with a multiline nonlinear least square fit, but even in such cases, the eigenvalues can still be determined to high accuracy from the single line fit expression (22). The single line fit is reviewed in the Appendix.

4. Computation of Eigenfunctions

If both sides of Eq. (13) are multiplied by $T^{-1}w(t)\exp(iEt)$ and integrated from 0 to T, the result is

$$\psi(x,y,E)=\frac{1}{T}\int_0^T \psi(x,y,t)\, w(t)\exp(iEt)\, dt$$
$$=\sum_{n,j} A_{nj}u_{nj}(x,y)\,\mathscr{L}_1(E-E_n), \tag{23}$$

where the integration is to be interpreted as numerical using the trapezoidal rule.

The function $\psi(x,y,E)$ will exhibit a maximum whenever $E=E_n$. If $E_{n'}$ is a particular member of the set E_n, $\psi(x,y,E_{n'})$ can be written

$$\psi(x,y,E_{n'})=\sum_j A_{n'j}u_{n'j}(x,y)\,\mathscr{L}_1(0)+\sum_{n,j}{}' A_{nj}u_{nj}(x,y)\,\mathscr{L}_1(E_{n'}-E_n), \tag{24}$$

where the prime on the second summation implies omission of terms corresponding to $n = n'$.

For negligible overlap between the resonant terms in Eq. (23), the second summation in Eq. (24) can be neglected, and to an excellent approximation one has

$$\psi(x, y, E_n) = \sum_j A_{nj} u_{nj}(x, y)\, \mathscr{L}_1(0). \tag{25}$$

If one chooses the initial wavefunction $\psi(x, y, 0)$ so that at most one member of a degenerate set of states is excited at one time, the numerical computation of a particular eigenfunction $u_n(x, y)$ reduces to the numerical integration

$$u_n(x, y) = \text{const} \times \int_0^T \psi(x, y, t)\, w(t) \exp(iE_n t)\, dt = \text{const} \times \psi(x, y, E_n). \tag{26}$$

Generation of the eigenfunctions by means of Eq. (26) requires prior knowledge of the energy eigenvalues and consequently one or more additional time dependent solutions of the Schrödinger equation. The number depends on computer storage available for the eigenfunctions that are generated simultaneously with $\psi(x, y, t)$. Obviously, storage requirements are the least stringent for one-dimensional problems and a large number of eigenfunctions can be generated simultanously in a single computer run.

Tests have shown that eigenfunctions computed in this manner are exceedingly accurate [11, 15]. Diagonal matrix elements for a harmonic oscillator potential can be computed to an accuracy of one part in 10^6 using wavefunctions constructed in this manner [11]. Recently, Davis and Heller used an expression similar to Eq. (26) with a $\psi(x, y, t)$ determined from semi-classical considerations to generate individual eigenfunctions [18].

5. Further Computational Considerations

There is as yet little concrete information on the relative computational efficiencies of the spectral method and matrix diagonalization. A few general comments, however, are in order.

In applying the procedure to the determination of energy eigenvalues, a preponderant fraction of the computer time goes to the generation of the time-dependent wavefunction by Eqs. (4)–(8). Equivalently, for a little more than the price of solving the time-dependent Schrödinger equation, the energies and probabilities of the component stationary states in a time-dependent wave packet can be determined. Since most of the computer time for advancing the time-dependent solution is invested in FFT computations, the computation time for the overall calculation scales as $\sim MN^k \ln N$, where M is the number of time steps, k is the number of space dimensions required for the problem, and N^k is the number of grid points. In general, M is determined by the desired resolution of the energy levels and does not vary with

the dimensionality of the problem. The number N^* of plane wave basis states used in the calculation is equal to the number of grid points. Consequently, computer time must scale with the number of basis states as $\sim MN^* \ln N^*$.

If the same problem is formulated and solved by matrix diagonalization using the same set of plane wave basis states, the computation time must scale at least as the time required for diagonalizing the matrix, or as $\sim N^{*3}$, implying that for problems requiring large numbers of basis states, matrix diagonalization could become less efficient than the spectral method. For certain potentials, it is possible to employ basis functions that minimize the required number N^*, and there may be little or no relative penalty for having to perform $\sim N^{*3}$ numerical operations. If one approaches the task of setting up a general computational scheme applicable to a wide variety of potentials, on the other hand, it becomes necessary to fix on a particular set of basis functions. In this more general case, the $\sim N^{*3}$ numerical operations can result in a relative computational penalty. In addition, computation of the matrix elements can become an important factor in the overall time required.

In conclusion, the relative computational efficiencies of the spectral and matrix diagonalization techniques can be expected to be problem dependent. The main attraction of the spectral method is that it is applicable with comparable efficiency and accuracy to a wide class of potential functions.

6. 1-D Asymmetric Double Well Potential

A potential of the form

$$V(x) = k_0 - k_2 x^2 + k_3 x^3 + k_4 x^4 \tag{27}$$

was used to describe an asymmetric double well potential in [2, 16, 17]. Computations with the spectral method were made for this potential and the parameter values $k_0 = -132.7074997$, $k_2 = +7$, $k_3 = 0.5$, $k_4 = 1$, corresponding to one of the cases treated in the above papers. The constant k_0 was selected to give a zero value to the potential for $x = x_1 = 3.813$ and $x = x_2 = -4.112$. This constant value was continued for $x > x_1$, and $x < x_2$. The resulting potential is a finite well that replaces the unbounded potential of (27). The depth of the potential well was selected to satisfy criterion (11) for the time step $\Delta t = 5.73$. A plot of the potential is displayed in Fig. 1, overlaid with a plot of the initial wavefunction

$$\psi(x, 0) = \exp[-(x-a)^2/2\sigma^2] + \exp[-(x+a)^2/2\sigma^2], \tag{28}$$

where $a = 1.9$ and $\sigma = 0.87$. The cutoff of the potential can affect the energy eigenvalues for one or two levels near the top of the well but otherwise has a negligible effect on the remaining bound states. The value $M = \frac{1}{2}$ was used in conformity with [17].

The time-dependent solution to the Schrödinger equation was generated over 16,384 increments in time. A computation with twice as many increments left the

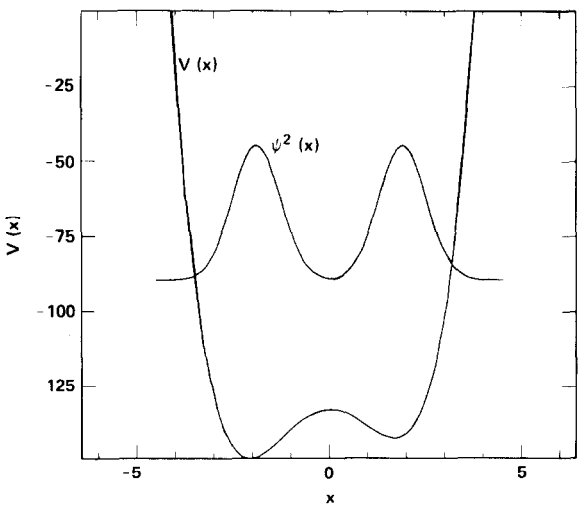

FIG. 1. Plot of 1-D asymmetric double well potential and initial wavefunction used to generate energy spectrum.

energy eigenvalues unchanged to seven significant figures. The computational grid contained 512 points with $\Delta x = 0.825$. Computation with 256 grid points resulted in changes of the energy eigenvalues in the seventh significant figure. Since this example was intended as an illustration, no attempt was made to optimize with respect to running time and accuracy. Acceptable accuracy for most applications could be obtained with far fewer time and space increments.

The resulting energy spectrum is displayed in Fig. 2, which shows a total of 27

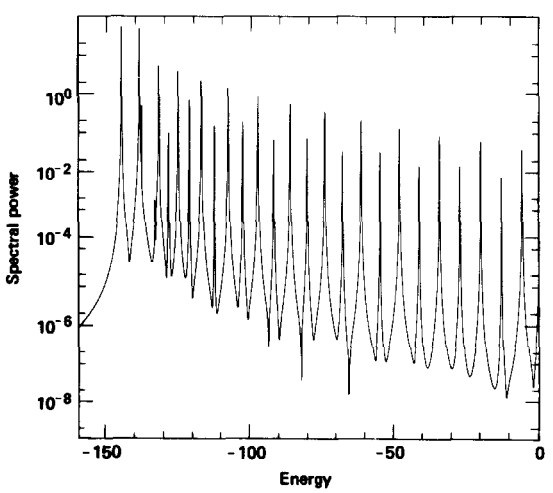

FIG. 2. Energy spectrum of bound states of asymmetric double well potential.

bound levels. The energy eigenvalues are listed in Table I together with values for the same potential from [2, 16, 17] where available. The eigenvalues determined by the spectral method are also listed in reduced form with the origin shifted to correspond with those of [17], which locates the zero in the potential at the top of the hump between the two wells.

The eigenvalues in [2] were calculated with a limited basis set of only 20 harmonic oscillator eigenfunctions. As a result, great accuracy is not expected. In [16], the number of harmonic oscillator basis functions was increased to 30, which improves accuracy substantially. Agreement between [16] and the spectral method results is good for the four lowest order levels, but becomes successively worse with increasing order after that. Computation in [17] is based on a combination power series and WKB solution. The authors of [17] claim accuracy in three to five places after the

TABLE I

Energy Eigenvalues E_n for Asymmetric Double Well Potential

				Spectral method	
n	Ref. 2(SH)	Ref. 16(PS)	Ref. 17(ZT)	Reduced	Unreduced
0	−12.2550	−12.2585	−12.258824	−12.258438	−144.96594
1	−6.0450	−6.0455	−6.045688	−6.045418	−138.75331
2	−5.265	−5.286	−5.287076	−5.286089	−137.66686
3	−0.625	−0.646	−0.647054	−0.646627	−133.35413
4	0.735	0.692	0.689775	0.691204	−132.01629
5	4.210	4.059	4.051291	4.053229	−128.65342
6	7.55	7.3785	7.364894	7.368937	−125.33856
7	11.85	11.2665	11.227179	11.235521	−121.47198
8	16.70	15.5125	15.413241	15.431918	−117.27558
9	—	—	—	19.938752	−112.76882
10	—	—	—	24.722016	−107.98548
11	—	—	—	29.758660	−102.94872
12	—	—	—	35.029816	−97.67768
13	—	—	—	40.519900	−92.18760
14	—	—	—	46.215701	−86.49180
15	—	—	—	52.105824	−80.60168
16	—	—	—	58.180283	−74.52721
17	—	—	—	64.430175	−68.27733
18	—	—	—	70.847383	−61.86011
19	—	—	—	77.424233	−55.28325
20	—	—	—	84.152963	−48.55450
21	—	—	—	91.024978	−41.68244
22	—	—	—	98.029195	−34.67820
23	—	—	—	105.149081	−27.55811
24	—	—	—	112.356276	−20.35076
25	—	—	—	119.592224	−13.11431
26	—	—	—	126.704585	−6.00153

Note. Comparison between spectral method, Ref. [2](SH), Ref. [16](PS), and Ref. [17](ZT).

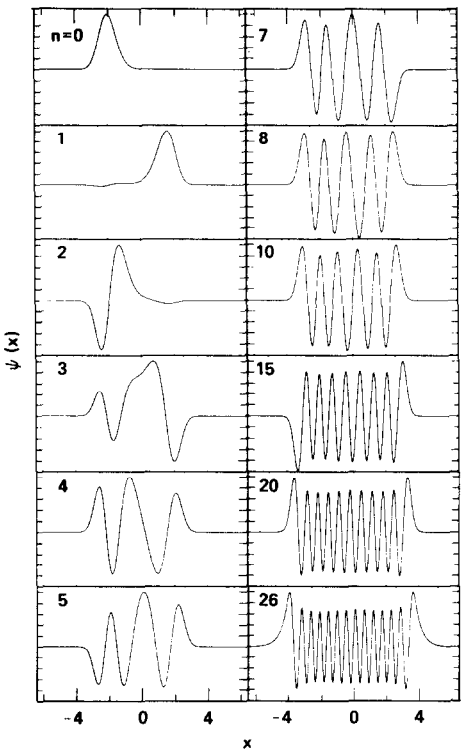

FIG. 3. Selected eigenfunctions for asymmetric double well potential.

decimal point. The agreement with the spectral method is this good for the lowest two levels only. Agreement is to at least three significant figures throughout, however.

Figure 3 shows selected eigenfunctions calculated using Eq. (26). The lower order eigenfunctions in Fig. 3 resemble closely their counterparts in [2, 17].

7. HÉNON–HEILES POTENTIAL

We turn our attention next to the Hénon–Heiles potential which has the following form in Cartesian coordinates:

$$V(x,y) = \tfrac{1}{2}M(\omega_1^2 x^2 + \omega_2^2 y^2) + \lambda x(y^2 - \tfrac{1}{3}x^2). \tag{29}$$

For $M = 1$ and $\omega_1 = \omega_2 = 1$, the potential (29) becomes in polar coordinates

$$V(r) = r^2/2 - (\lambda/3)\, r^3 \cos 3\theta. \tag{30}$$

Energy eigenvalues and eigenfunctions were determined with the spectral method for $\lambda = 0.1118034$, corresponding to a dissociation energy $V_0 = 13.3333$. Energy

eigenvalues for this potential were previously determined by matrix diagonalization and can be found in [3–6].

A contour plot of the potential (30) is shown in Fig. 4a. The spectral method, however, requires a cutoff, which was imposed at 25 percent above the dissociation energy. A contour plot of the bounded potential used in the computations is shown in Fig. 4b.

Computations were made on a 128×128 grid of length $L_0 = 12.5$. The time-dependent solution of the Schrödinger equation was advanced in increments $\Delta t = 0.025$.

A. Symmetry Conditions and the Choice of Initial Wave Functions

The complete spectrum of energy levels below the dissociation energy, computed from an initial wavefunction composed of randomly phased plane waves is shown in Fig. 5. The number of integration steps is 8192. Unfortunately, this spectrum is not suitable for an accurate determination of all of the desired eigenvalues. Some of the lines in this spectrum really represent overlapping resonances that result from the narrow splitting of degenerate levels of the harmonic oscillator. Although the

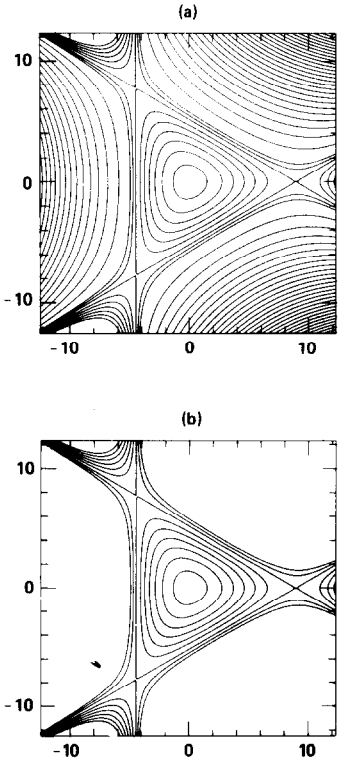

FIG. 4. Contour plot of (a) Hénon–Heiles potential, (b) Hénon–Heiles potential cutoff at twenty-five percent above the dissociation energy used for computations.

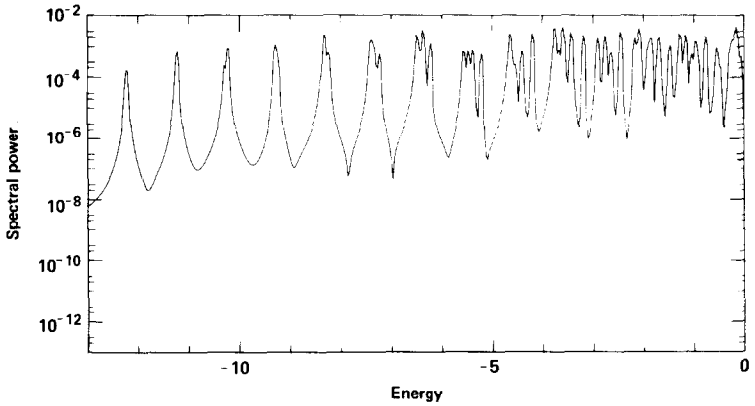

FIG. 5. Energy spectrum excited by random superposition of plane waves for stationary states of Hénon–Heiles potential below the dissociation energy.

resolution of such a spectrum can always be enhanced by developing the numerical solution to the Schrödinger equation over a longer time, it is more profitable to make multiple runs with initial wave functions of selected symmetry to avoid the simultaneous excitation of closely spaced energy levels. We thus turn our attention to the symmetry properties of the potential (Eq. (30)) and the corresponding wavefunction. Although much of the following exposition represents a recapitulation of the properties of the group C_{3v}, which is a symmetry group of the potential of Eq. (30), its completeness is essential to properly explain the choice of initial conditions for the time-dependent Schrödinger equation.

Clearly, the Hamiltonian of (30) is invariant under a rotation of $2\pi/3$ in θ. If $\mathscr{R}$ is an operator such that $\mathscr{R}\psi(r, \theta) = \psi(r, \theta + 2\pi/3)$, $\mathscr{R}$ and H must commute, and it is possible to find simultaneous eigenfunctions of $\mathscr{R}$ and H. Furthermore, the eigenvalues of $\mathscr{R}$ satisfy the relation $R^3 = 1$, or $R = 1, \exp(\pm i2\pi/3)$. Straightforward analysis shows that the eigenfunctions of the Schrödinger equation must therefore have the following general form:

$$\begin{aligned} u_1(\theta) &= f_1(\theta) + f_1(\theta + 2\pi/3) + f_1(\theta - 2\pi/3), \\ u_+(\theta) &= f_+(\theta) + f_+(\theta + 2\pi/3)\, e^{-i2\pi/3} + f_+(\theta - 2\pi/3)\, e^{i2\pi/3}, \\ u_-(\theta) &= f_-(\theta) + f_-(\theta + 2\pi/3)\, e^{i2\pi/3} + f_-(\theta - 2\pi/3)\, e^{-i2\pi/3}, \end{aligned} \tag{31}$$

where for simplicity the dependence on r has been suppressed. Here

$$\mathscr{R}u_1(\theta) = u_1(\theta), \qquad \mathscr{R}u_+(\theta) = e^{i2\pi/3}u_+(\theta), \qquad \mathscr{R}u_-(\theta) = e^{-i2\pi/3}u_-(\theta). \tag{32}$$

If $f_1(\theta)$ is expressed as a Fourier series

$$f_1(\theta) = \sum_l f_{1l}\, e^{il\theta}, \tag{33}$$

$u_1(\theta)$ is expressible as

$$u_1(\theta) = \sum_l (3f_{1\,3l})\, e^{i3l\theta}. \tag{34}$$

Similarly, if

$$f_+(\theta) = \sum_l f_{+\ l} e^{il\theta}, \tag{35a}$$

$$f_-(\theta) = \sum_l f_{-\ l} e^{il\theta}, \tag{35b}$$

then $u_+(\theta)$ and $u_-(\theta)$ are expressible as

$$u_+(\theta) = \sum_l (3f_{+\ 3l+1})\, e^{i(3l+1)\theta}, \qquad u_-(\theta) = \sum_l (3f_{-\ 3l-1})\, e^{i(3l-1)\theta}. \tag{36}$$

The Hamiltonian of (30) is also invariant under reflection through the x axis.

Let this reflection operator be called σ_v. If $u_n(r, \theta)$ is an eigenfunction satisfying the Schrödinger equation, $\sigma_v u_n(r, \theta) = u_n(r, -\theta)$ also satisfies the Schrödinger equation with the same energy eigenvalue. If $f_1(\theta)$ is chosen either even or odd, $u_1(\theta)$ is an eigenfunction of σ_v with eigenvalues ± 1, respectively, or

$$\sigma_v u_1(\theta) = \pm u_1(\theta). \tag{37}$$

If $f_+(\theta)$ and $f_-(\theta)$ are either both even or both odd, one obtains

$$\sigma_v u_\pm(\theta) = \mp u_\mp(\theta). \tag{38}$$

If $f_+(\theta)$ and $f_-(\theta)$ are neither even nor odd, it is clear that $\sigma_v u_+$ and $\sigma_v u_-$ must be representable as a linear combination of $u_+(\theta)$ and $u_-(\theta)$. In either case, the behavior of $u_+(\theta)$ and $u_-(\theta)$ under application of σ implies that these sets of states are doubly degenerate.

We can thus generate all energy eigenvalues in three separate runs with the initial wavefunction chosen to have the following forms: (a) $u_1(r, \theta)$ with $f_1(r, \theta)$ even, (b) $u_1(r, \theta)$ with $f_1(r, \theta)$ odd, (c) either $u_+(r, \theta)$ or $u_-(r, \theta)$. In this manner, all of the states of the three important symmetry types can be excited separately and the overlap of narrowly split degenerate levels can be avoided. Equations (34) and (36) serve as a model for the initial wavefunctions. The actual excitation functions used were

$$\psi_{1e}(r, \theta, 0) = \exp(-r^2/2\sigma^2) \sum_{n=0}^{4} (r/\sigma)^{3l} N_{3l} \cos 3l\theta, \tag{39a}$$

$$\psi_{1o}(r, \theta, 0) = \exp(-r^2/2\sigma^2) \sum_{l=0}^{4} (r/\sigma)^{3l} N_{3l} \sin 3l\theta, \tag{39b}$$

$$\psi_+(r, \theta, 0) = \exp(-r^2/2\sigma^2) \sum_{l=0}^{4} (r/\sigma)^{3l+1} N_{3l+1} \exp[i(3l+1)\theta], \tag{39c}$$

where $\sigma = 1.5$ and

$$N_l = (2^l l!)^{-1/2} \tag{40}$$

is a normalization coefficient. Functions (39a)–(39c) are chosen to have the same form in the limit $r \to 0$ as solutions to the Schrödinger equation for a harmonic oscillator potential, namely,

$$u_{nl}(r, \theta) = \exp(il\theta) \exp(-r^2/2\sigma^2)(r/\sigma)^l L_n^l(r^2/\sigma^2), \tag{41}$$

where $L_n^l(r^2, \sigma^2)$ is a generalized Laguerre polynomial.

B. Energy Eigenvalues

Figure 6 shows the energy spectra for states of the three symmetry types resulting from excitation by the initial wave functions (39a)–(39c). Energy eigenvalues computed in runs of 16,384 steps are listed in Table II, in addition to corresponding values from [4–6]. Each run required 13 minutes of time on a CRAY 1 computer.

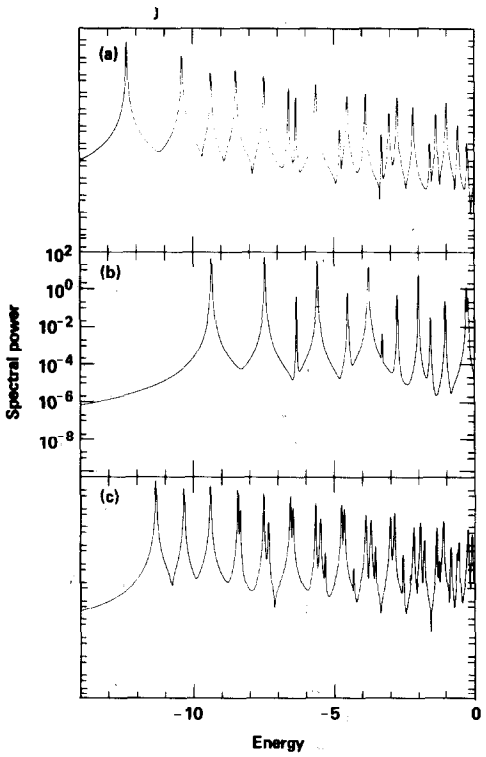

FIG. 6. Energy spectra for Hénon–Heiles potential below the dissociation energy for states of three main symmetries (a) $R = 1$, $\sigma_v = 1$; (b) $R = 1$, $\sigma_v = -1$; (c) $R = \exp(i2\pi/3)$, $\exp(-i2\pi/3)$ (degenerate states).

TABLE II

Energy Eigenvalues for the Hénon–Heiles Potential

Quantum numbers n	l	Ref. [4](NM) Ref. [6](NKTM)	Ref. 5 (DH)	Spectral method
0	0	0.9986	0.9986	0.9986
1	1	1.9901	1.9901	1.9901
2	0	2.9562	2.9562	2.9563
	2	2.9853	2.9853	2.9854
3	1	3.9260	3.9260	3.9261
	3	3.9824	3.9824	3.9825
	−3	3.9858	3.9858	3.9859
4	0	4.8702	4.8701	4.8703
	2	4.8987	4.8986	4.8988
	4	4.9863	4.9863	4.9864
5	1	5.8170	5.8170	5.8172
	3	5.8670	5.8670	5.8672
	−3	5.8815	5.8814	5.8816
	5	5.9913	5.9913	5.9915
6	0	6.7379	6.7379	6.7381
	2	6.7649	6.7649	6.7650
	4	6.8534	6.8534	6.8538
	−6	6.9989	6.9989	6.9991
	6	6.9994	6.9994	6.9996
7	1	7.6595	7.6595	7.6597
	3	7.6977	7.6977	7.6979
	−3	7.7369	7.7369	7.7371
	5	7.8327	7.8327	7.8329
	7	8.0094	8.0094	8.0096
8	0	8.5541	8.5540	8.5542
	2	8.5764	8.5764	8.5765
	4	8.6779	8.6779	8.6782
	−6	8.8113	8.8113	8.8116
	6	8.8152	8.8152	8.8154
	8	9.0217	9.0217	9.0220
9	1	9.444	9.4441	9.4442
	3	9.467	9.4668	9.4670
	−3	9.552	9.5524	9.5526
	5	9.629	9.6294	9.6296
	7	9.794	9.7941	9.7944
	−9	10.0354	10.0354	10.0356
	9	10.0356	10.0356	10.0359
10	0	10.3052	10.3051	10.3053
	2	10.318	10.3184	10.3185
	4	10.463	10.4636	10.4637
	−6	10.573	10.5729	10.5727
	6	10.590	10.5905	10.5907
	8	10.774	10.7740	10.7742

Table continued

TABLE II (*Continued*)

Quantum numbers n	l	Ref. [4](NM) Ref. [6](NKTM)	Ref. [5](DH)	Spectral method
	10	11.0497	11.0497	11.0500
11	1	11.152	11.1518	11.1517
	3	11.160	11.1603	11.1603
	−3	11.325	11.3259	33.3253
	5	11.383	11.3835	11.3831
	7	11.534	11.5337	11.5337
	9	11.750	—	11.7497
	−9	11.752	—	11.7525
	11	11.968	—	11.9679
12	0	11.966	—	11.9659
	2	12.065	—	12.0651
	4	12.206	—	12.2054
	6	12.334	—	12.3335
	−6	12.277	—	12.2771
	8	12.480	—	12.4801
	10	12.712	—	12.7116
	12	12.748	—	12.7474
	−12	13.052	—	13.0310
13	1	12.762	—	12.7609
	3	13.077	—	13.0772
	−3	13.087	—	13.0868
	5	13.081	—	13.0800
	7	13.233	—	13.2319

Note. Comparison between Ref. [4](NM) (four figures after decimal), Ref. [6](NKTM) (three figures after decimal), Ref. [5](DH), where available, and spectral method.

The large number of steps were computed to ensure the resolution of some closely spaced states near dissociation. The computations in [4], which took advantage of the tridiagonal structure of the Hamiltonian matrix, were based on sets of 406 and 595 basis states, and the computations in [6] required sets of 990 and 1225 basis states.

The ordering of the eigenvalues is analogous to the conventional ordering of the states of a two-dimensional harmonic oscillator. This ordering principle becomes less physically meaningful for the higher order states most affected by the perturbing term in Eq. (30), but it nonetheless serves as a classification scheme.

The states with values of l equal to zero or a multiple of three are generated with Eqs. (39a) and (39b). The $+l$ and $-l$ values that are multiples of three are arbitrarily assigned to the states with even and odd symmetry, i.e., to those originating from Eq. (39a) and Eq. (39b), respectively. States with the remaining l values are generated with Eq. (39c). Energy eigenvalues are assigned a principle quantum number n and angular quantum number l in accordance with the hierarchy of states of the two-dimensional harmonic oscillator. Where harmonic oscillator states for more than one l value are degenerate, the highest eigenvalue is assigned to the highest l value. Our

classification scheme is in almost complete agreement with that employed in [4, 6]. The only exceptions are the interchange of states ($n = 12$, $l = \pm 12$), with states ($n = 13$, $l = \pm 3$), and state ($n = 11$, $l = 11$) with state ($n = 12$, $l = 2$).

All three eigenvalue sets listed in Table II are in very close agreement. Where [4, 5] agree to four figures after the decimal place, the spectral method results are consistently higher by 1 to 3 in the fourth figure after the decimal. It should be stressed, however, that the spectral method is based upon numerical solutions for the wavefunction, whereas Hamiltonian matrix elements are available in analytic form for the Hénon–Heiles potential, which eliminates one source of approximation error in the matrix diagonalization approach. In any case, the high accuracy achieved by the spectral method for the Hénon–Heiles potential should be attainable for suitably well-behaved potentials whose corresponding Hamiltonian matrices are not expressible in simple analytic and/or tridiagonal form.

C. *Wave Functions*

Contour plots of the square amplitude of selected wave functions calculated with Eq. (26) are shown in Figs. 7 and 8. The effect of the C_3 symmetry of the potential is

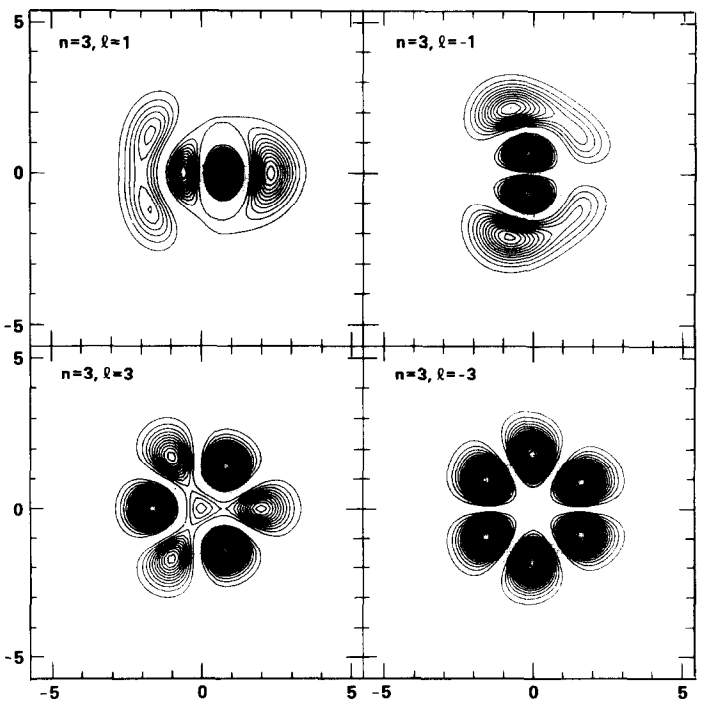

FIG. 7. Representative wavefunctions for states of Hénon–Heiles potential: contours of square amplitudes.

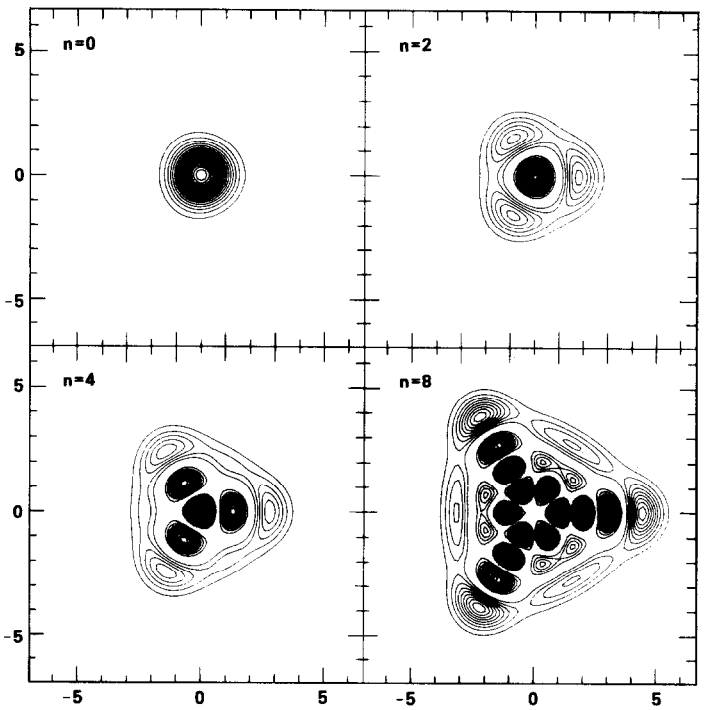

FIG. 8. Representative wavefunctions for states of Hénon–Heiles potential: contours of square amplitudes for $l = 0$ states.

evident. The distortion is most noticeable for the $l = 0$ wavefunctions whose contours would be circles if only the harmonic oscillator part of the potential were present. In Fig. 8, we see the progressive deformation of $l = 0$ wavefunctions with increasing values of the principal quantum number n.

8. Summary and Conclusion

We have described a new method for determining the eigenvalues and eigenfunctions of the Schrödinger equation. This new method, which we have called the spectral method, relies on a kind of numerical spectroscopy for extracting the eigenvalues from correlation data. The latter are obtained by solving the time-dependent Schrödinger equation using the split operator FFT method and correlating the time-dependent wavefunction with the initial wavefunction. States of particular symmetry can be isolated and studied by properly choosing the initial wavefunction for the calculation. Such a procedure is useful for distinguishing states with very closely spaced energy eigenvalues. In sample calculations, the accuracy of the spectral

method has been demonstrated to be comparable with that of the matrix diagonalization technique. The principal attraction of the spectral method, however, is that it can be applied to a general set of potentials with little variation in efficiency. It should be particularly useful for potentials that are specified numerically or that would require numerical integration for the evaluation of matrix elements.

Appendix: Lineshape Fitting Method

The lineshape function $\mathscr{L}_1(E - E_n)$ can be written

$$\mathscr{L}_1(\delta) = \mathscr{F}_1(\delta) - \tfrac{1}{2}[\mathscr{F}_1(\delta + 1) + \mathscr{F}_1(\delta - 1)], \tag{A1}$$

where

$$\mathscr{F}_1(\delta) = (\exp(2\pi i\delta) - 1)/2\pi i\delta, \qquad \mathscr{F}_1(0) = 1, \tag{A2}$$

and

$$\delta = (E - E_n)T/2\pi. \tag{A3}$$

Let us assume that a local maximum in the sampled values of $\mathscr{P}_1(E)$ occurs for $E_m = m\,\Delta E$, where ΔE is the sampling interval in the computation of the numerical Fourier transform $\mathscr{P}_1(E)$. In the range $(m-1)\,\Delta E \leqslant E \leqslant (m+1)\,\Delta E$, $\mathscr{P}_1(E)$ can, to an excellent approximation, be represented as

$$\mathscr{P}_1(E) = W_n \mathscr{L}_1(E - E_n), \tag{A4}$$

where E_n is the desired eigenvalue. Let the following ratio be formed from sampled values of $\mathscr{P}_1(E)$ in the neighborhood of E_m:

$$\mathscr{R}(\delta') = \mathscr{P}_1[(m+1)\,\Delta E]/\mathscr{P}_1[(m-1)\,\Delta E] = \mathscr{L}_1(\delta' + 1)/\mathscr{L}_1(\delta' - 1), \tag{A5}$$

where

$$\delta' = (E_m - E_n)\,T/2\pi. \tag{A6}$$

Making use of Eqs. (A2) and (A3), we can write Eq. (A5) as

$$(\delta'^2 - 3\delta' + 2)/(\delta'^2 + 3\delta' + 2) = R, \tag{A7}$$

or equivalently

$$\delta'^2 - 3\delta' r + 2 = 0, \tag{A8}$$

where

$$r = (1 + R)/(1 - R). \tag{A9}$$

The appropriate solution to Eq. (A8) is

$$\begin{aligned} \delta' &= (-3r + (9r^2 - 8)^{1/2})/2, \qquad R < 1, \\ &= (-3r - (9r^2 - 8)^{1/2})/2, \qquad R > 1. \end{aligned} \tag{A10}$$

In terms of the line-center offset parameter δ', E_n then can be determined from

$$E_n = E_n - 2\pi\delta'/T, \tag{A11}$$

and W_n can be obtained from

$$W_n = \mathscr{P}_1(m\,\Delta E)/\mathscr{L}_1(\delta'). \tag{A12}$$

REFERENCES

1. No attempt will be made to cite representative applications of this method, since it is so widespread. Matrix diagonalization, however, is the method used in [2–6].
2. R. L. SAMORJAI AND D. F. HORNIG, *J. Chem. Phys.* **36** (1962), 1980.
3. K. S. J. NORDHOLM AND S. A. RICE, *J. Chem. Phys.* **61** (1974), 203, 768.
4. D. W. NOID AND R. A. MARCUS, *J. Chem. Phys.* **67** (1977), 559.
5. M. J. DAVIS AND E. J. HELLER, *J. Chem. Phys.* **71** (1979), 3383.
6. D. W. NOID, M. L. KOSZYKOWSKI, M. TABOR, AND R. A. MARCUS, *J. Chem. Phys.* **72** (1980), 6169.
7. J. W. COOLEY, *Math. Comput.* **15** (1961), 363.
8. J. M. BLATT, *J. Comput. Phys.* **1** (1967), 382.
9. J. N. BASS, *J. Comput. Phys.* **9** (1972), 555.
10. M. D. FEIT AND J. A. FLECK, JR., *Appl. Opt.* **19** (1980), 1154.
11. M. D. FEIT AND J. A. FLECK, JR., *Appl. Opt.* **19** (1980), 2240.
12. M. D. FEIT AND J. A. FLECK, JR., *Appl. Opt.* **19** (1980), 3140.
13. M. D. FEIT AND J. A. FLECK, *J. Opt. Soc. Amer.* **17** (1981), 1361.
14. J. A. FLECK, JR., J. R. MORRIS, AND M. D. FEIT, *Appl. Phys.* **10** (1976), 129.
15. A successful application of the spectral method to a symmetric non-Hermitian operator yielded the complex eigenvalues and eigenfunctions for the unloaded optical resonator. M. D. FEIT AND J. A. FLECK, JR., *Appl. Opt.* **20** (1981), 2843.
16. E. A. PSHENICHNOV AND N. D. SOKOLOV, *Opt. Spectrosc.* (USSR) **17** (1964), 183 (*Opt. Spektrosk.* **17** (1964), 343).
17. N. I. ZHIRNOV AND A. V. TUREV, *Opt. Spectrosc.* (USSR) **47** (1980), 480 (*Opt. Spektrosk.* **47** (1979), 869).
18. M. J. DAVIS AND E. J. HELLER, *J. Chem. Phys.* **75** (1981), 3916.